Mid-Cenozoic tectonic and paleoenvironmental setting of the central Arctic Ocean

Matthew O'Regan,[1] Kathryn Moran,[1,2] Jan Backman,[3] Martin Jakobsson,[3] Francesca Sangiorgi,[4] Henk Brinkhuis,[4] Rob Pockalny,[1] Alasdair Skelton,[3] Catherine Stickley,[5] Nalan Koç,[5,6] Hans-Jürgen Brumsack,[7] and Debra Willard[8]

Received 17 October 2007; revised 28 January 2008; accepted 18 February 2008; published 26 March 2008.

[1] Drilling results from the Integrated Ocean Drilling Program's Arctic Coring Expedition (ACEX) to the Lomonosov Ridge (LR) document a 26 million year hiatus that separates freshwater-influenced biosilica-rich deposits of the middle Eocene from fossil-poor glaciomarine silty clays of the early Miocene. Detailed micropaleontological and sedimentological data from sediments surrounding this mid-Cenozoic hiatus describe a shallow water setting for the LR, a finding that conflicts with predrilling seismic predictions and an initial postcruise assessment of its subsidence history that assumed smooth thermally controlled subsidence following rifting. A review of Cenozoic tectonic processes affecting the geodynamic evolution of the central Arctic Ocean highlights a prolonged phase of basin-wide compression that ended in the early Miocene. The coincidence in timing between the end of compression and the start of rapid early Miocene subsidence provides a compelling link between these observations and similarly accounts for the shallow water setting that persisted more than 30 million years after rifting ended. However, for much of the late Paleogene and early Neogene, tectonic reconstructions of the Arctic Ocean describe a landlocked basin, adding additional uncertainty to reconstructions of paleodepth estimates as the magnitude of regional sea level variations remains unknown.

Citation: O'Regan, M., et al. (2008), Mid-Cenozoic tectonic and paleoenvironmental setting of the central Arctic Ocean, *Paleoceanography*, *23*, PA1S20, doi:10.1029/2007PA001559.

1. Introduction

[2] Our understanding of the geologic history of the Arctic Ocean has long been hampered by a lack of regional sediment archives extending beyond the most recent Pleistocene. In the absence of these records, the tectonic and paleoenvironmental evolution of the region has largely been derived from interpretations of remotely acquired geophysical data and supplemented with published information from industry wells and circumarctic outcrops. The only marine geologic record from the central Arctic Ocean available for ground truthing these interpretations was acquired during the Integrated Ocean Drilling Program (IODP) Expedition 302, the Arctic Coring Expedition (ACEX). These sediments were recovered from the Lomonosov Ridge (LR), a 1650 km long fragment of continental crust that extends from the Greenland to Siberian margins and divides the Arctic Ocean into the Mesozoic age Amerasian Basin and the Cenozoic age Eurasian Basin (Figure 1). The LR was rifted from the Barents-Kara shelf in the late Paleocene when seafloor spreading began along the Gakkel Ridge [*Vogt et al.*, 1979]. Although clear sets of marine magnetic anomalies in the Eurasian basin have allowed the lateral displacement of the LR to be traced through time [*Vogt et al.*, 1979; *Lawver et al.*, 2002; *Brozena et al.*, 2003; *Glebovsky et al.*, 2006], the lack of sediments to define its subsidence history has limited the ability of plate kinematic models to address the broader geodynamic evolution of the central Arctic Ocean.

[3] Drilling during ACEX penetrated 428 meters of sediment at four sites on the crest of the LR between 87° and 88°N. The sites were located 15 km apart along seismic line AWI-91090 [*Jokat et al.*, 1992] and drilled in water depths ranging from 1208 to 1290 m below sea level (mbsl) (Figure 2) [*Moran et al.*, 2006]. A coherent seismostratigraphy allowed the results to be combined to form a single composite section, with 78% core recovery in the upper 271 m and less than 50% in the remaining, underlying 157 m [*Expedition 302 Scientists*, 2006]. At one site (M0004A), coring continued across a regional unconformity separating Cenozoic (56.2 Ma) from Mesozoic (~80 Ma) sediments [*Backman et al.*, 2008] (Figure 2). The recovery of the highly disturbed sample of Cretaceous age muds and sands from beneath this unconformity describe a shallow

[1]Graduate School of Oceanography, University of Rhode Island, Narragansett, Rhode Island, USA.
[2]Department of Ocean Engineering, University of Rhode Island, Narragansett, Rhode Island, USA.
[3]Department of Geology and Geochemistry, Stockholm University, Stockholm, Sweden.
[4]Palaeoecology, Laboratory of Palaeobotany and Palynology, Institute of Environmental Biology, Utrecht University, Utrecht, Netherlands.
[5]Norwegian Polar Institute, Polar Environmental Center, Tromsø, Norway.
[6]Department of Geology, University of Tromsø, Tromsø, Norway.
[7]Institut für Chemie und Biologie des Meeres, Oldenburg University, Oldenburg, Germany.
[8]U.S. Geological Survey, Reston, Virginia, USA.

0883-8305/08/2007PA001559

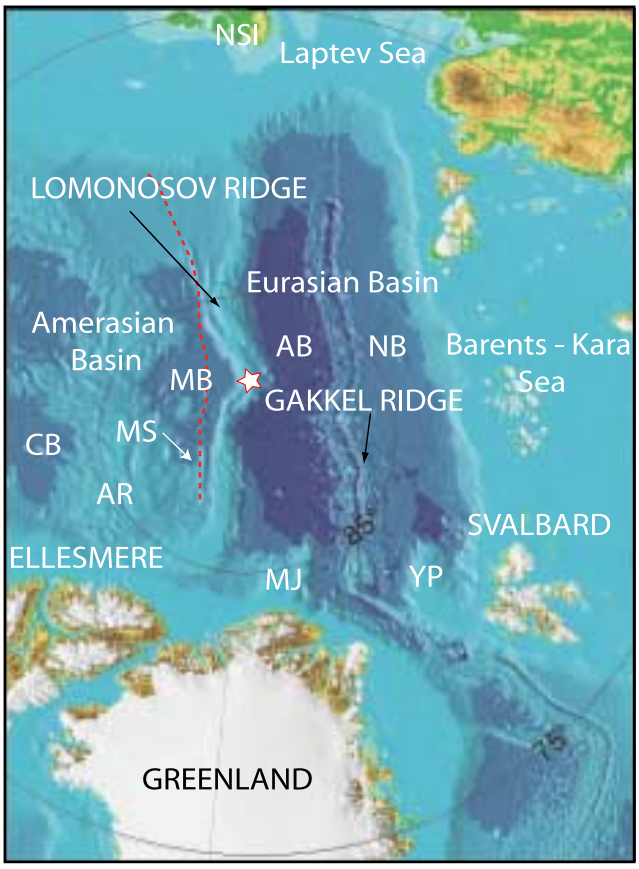

Figure 1. Annotated map of the central Arctic Ocean. Red dotted line outlines possible extent of continental crust associated with the Lomonosov Ridge in the Amerasian Basin. Abbreviations are AB, Amundsen Basin; AR, Alpha Ridge; CB, Canada Basin; MB, Makarov Basin; MJ, Morris Jesup Rise; MS, Marvin Spur; NB, Nansen Basin; NSI, New Siberian Islands; and YP, Yermak Plateau. Bathymetry is from the International Bathymetric Chart of the Arctic Ocean [*Jakobsson et al.*, 2000].

water environment [*Expedition 302 Scientists*, 2006]. Drilling results thus confirmed that this seismically recognized unconformity [*Jokat et al.*, 1992, 1995], marking the base of Tertiary age sediments was erosional [*Jakobsson et al.*, 2006], and likely formed during the rifting process that separated the LR from the Barents-Kara shelf. Hereinafter we refer to this feature as the rifting unconformity.

[4] In addition to the rifting unconformity, the presence of a 26 Ma long hiatus separating middle Eocene from early Miocene sediments was identified in the ACEX record [*Backman et al.*, 2008]. Although initial age control was poor, the hiatus was originally attributed to erosion/nondeposition caused by internal waves while the crest of the LR subsided from 550 to 1050 mbsl [*Moore and the Expedition Scientists*, 2006]. More recent micropaleontological, sedimentological and geochemical results reveal a shallow, freshwater dominated setting with an enrichment of terrestrial palynomorphs in sediments bounding this hiatus, indicating that the crest of the LR was at or near sea level during this time [*Sangiorgi et al.*, 2008]. By synthesizing these new results, we present a revised subsidence history for this segment of the LR and address two fundamental questions. The first is how to explain a shallow water setting for the LR more than 30 Ma after rifting ended, and the second is what triggered the rapid early Miocene onset of subsidence. Using published geophysical, structural and kinematic data, we argue that documented compressional forces provide a mechanism to explain the anomalous subsidence pattern observed at the ACEX sites and discuss the possible lateral extent of this hiatus.

2. Structure and Sedimentary Cover of the LR

[5] A single seismic refraction profile collected from a drifting ice island during the Canadian Lomonosov Ridge Experiment (LOREX) in 1979 [*Weber*, 1979] (Figure 3) provides one of the few constraints on the deeper crustal structure of the central LR. In close proximity to the ACEX drill sites, the upper crust has a thickness of 5 km and a velocity of 4.7–5.2 km/s, and the lower crust exceeds 20 km thick with a velocity of 6.6 km/s [*Mair and Forsyth*, 1982; *Forsyth and Mair*, 1984]. On the basis of these results, the Moho beneath the central LR is estimated to be at a depth of 25–28 km [*Forsyth and Mair*, 1984; *Weber and Sweeney*, 1985]. Seismic and gravity modeling following LOREX confirmed earlier calculations based on plumb line deflections that assumed the LR to be a sliver of isostatically equilibrated continental crust [*Weber and Sweeney*, 1990].

[6] As a double-sided passive margin [*Jokat et al.*, 1992], the LR has undergone at least two phases of extension associated with the Mesozoic opening of the Amerasian Basin, and the Cenozoic opening of the Eurasian Basin. Along the Eurasian flank, structural observations describe a series of rotated fault blocks that step down into the Amundsen Basin where a sharp gravity gradient marks their seaward extent and the beginning of clear marine magnetic anomalies [*Jokat et al.*, 1992; *Jokat and Micksch*, 2004; *Cochran et al.*, 2006]. These observations are consistent with structural features of nonvolcanic orthogonally rifted continental margins [*Cochran et al.*, 2006]. The Amerasian flank of the LR is less well defined. Gravimetric, bathymetric and seismic reflection data all indicate that the outer limit of the LR increases in width toward the Siberian margin [*Jokat*, 2005; *Cochran et al.*, 2006]. Connecting the outer Marvin Spur with the bathymetric/gravimetric boundary on the Siberian margin side of the North Pole, *Cochran et al.* [2006] suggested that the resulting arc defined a transform margin marking the seaward limit of the LR during the Mesozoic rotational opening of the Canada Basin (Figure 3).

[7] In line with the early observations from the 1960s and 1970s, from 85°N of Greenland to ~86°N of the Siberian margin, a single flat-crested feature broadly defines the structure of the LR [*Weber and Sweeney*, 1985; *Jokat*, 2005; *Cochran et al.*, 2006]. Coring during ACEX was conducted on this segment. Although described as monolithic, there are a series of unique structural characteristics

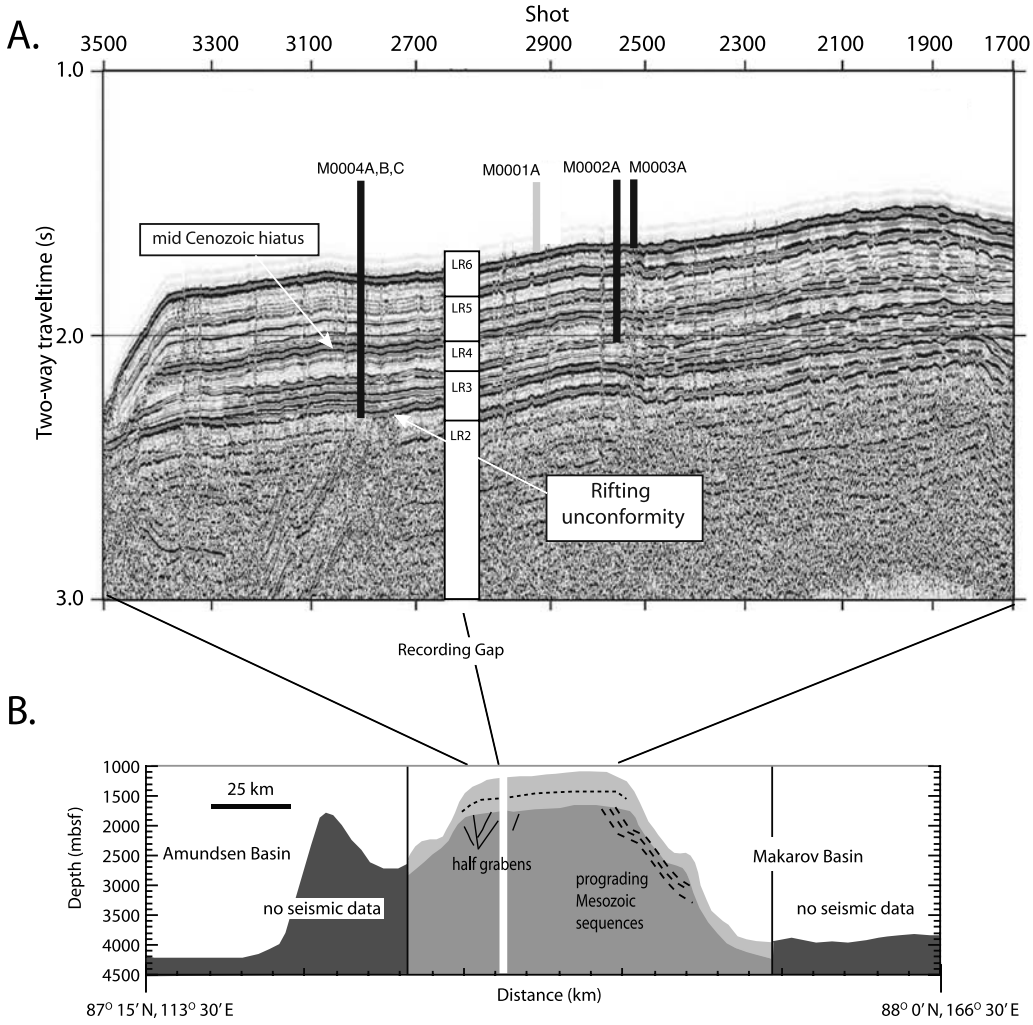

Figure 2. (a) ACEX-cored four sites on the LR located along seismic reflection profile AWI-91090 [*Jokat et al.*, 1992]. Core-seismic integration [*Jakobsson et al.*, 2006; *Backman et al.*, 2008] identified the location of the Cenozoic-Mesozoic and the mid-Cenozoic hiatus and allows comparison with the seismic units from *Jokat et al.* [1995]. Sonobouy-modeled velocities of these units are LR6 = 1.8 km/s; LR5 = 1.8 km/s; LR4 = 2.0 km/s; LR3 = 2.2 km/s; and LR2 = 4 km/s [*Jokat et al.*, 1995]. (b) Bathymetric profile running from the Makaraov to Amundsen Basin and crossing the LR along seismic profile AWI-91090. Bathymetry is from the International Bathymetric Chart of the Arctic Ocean [*Jakobsson et al.*, 2000]. Interpretation of Cenozoic sedimentary cover imaged by AWI-91090 shown in light grey with select sedimentary and structural features [after *Jokat et al.*, 1992, 1995; *Kristoffersen et al.*, 2007]. Dark grey shading indicates basement rocks or sediments older than the Cenozoic. Light grey shading indicates Cenozoic sediments. Stratigraphic interpretations only extend the length of the seismic profile.

between the North Pole and 85°N on the Siberian margin side of the LR. The first is a prominent bend in the strike of the LR that appears to be inherited from the initial rifting geometry and is mirrored in both the strike of the Gakkel Ridge and the conjugate Barents-Kara shelf [*Vogt et al.*, 1979; *Brozena et al.*, 2003; *Glebovsky et al.*, 2006]. Concomitant with this bend is a deeper subbasin running parallel to the strike of the LR. *Cochran et al.* [2006] argue that this subbasin represents an oblique nontransform offset that occurred as rifting along the eastern Gakkel Ridge stalled or slowed prior to marine magnetic anomaly 22 (C22) time. The bend in the LR is followed by a broad double-terraced feature that steps down into the Eurasian Basin beginning near 88°N on the Siberian margin side of the North Pole (Figure 3). This terrace is 50 km wide and located between 2200 and 3000 mbsl [*Cochran et al.*, 2006] and likely formed from extension during rifting of the Eurasian Basin. Finally, the segment from the North Pole to 86°N is also flanked and partially underlain by the lowest gravity anomalies observed along strike of the LR (Figure 3).

[8] Seismically, the boundary between Mesozoic (prerift and synrift) and Cenozoic (postrift) sediments on the LR is

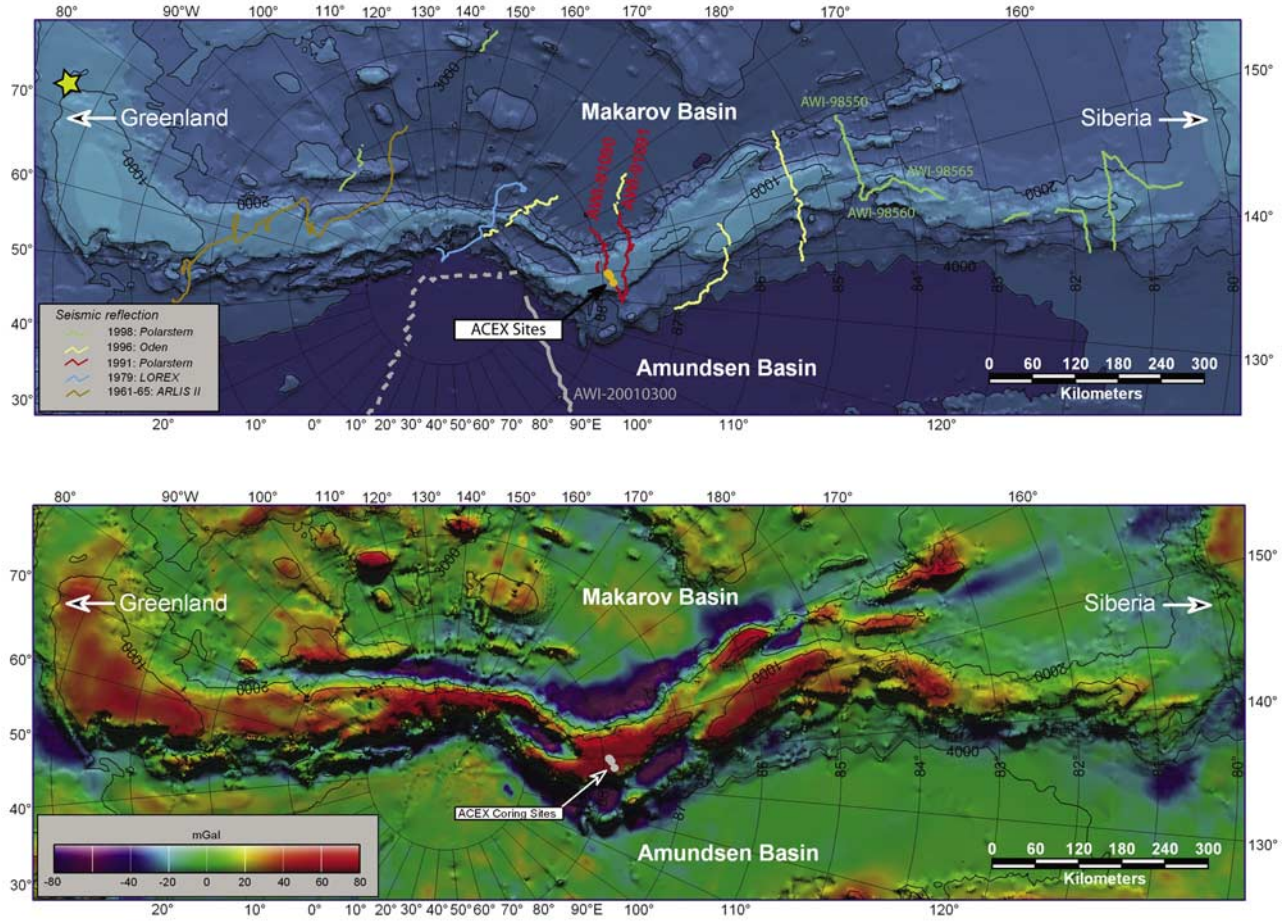

Figure 3. (top) Bathymetric map of the LR showing select geophysical data discussed in this paper. Bathymetry is from the International Bathymetric Chart of the Arctic Ocean [*Jakobsson et al.*, 2000]. Grey lines represent approximate positions of seismic lines from the Amundsen Basin: solid [*Jokat et al.*, 1995], doted [*Jokat and Micksch*, 2004]. Star indicates approximate position of the seismic lines from *Kristoffersen and Mikkelsen* [2006]. The other seismic lines and their references are 1991 (ARK-V111/3) [*Fütterer*, 1992; *Jokat et al.*, 1992, 1995]; 1996 (ARK-XII/1) [*Kristoffersen et al.*, 1997, 2001]; and 1998 (ARK-XIV/1a) [*Jokat*, 2005]. (bottom) Free air gravity anomalies of the LR showing lows that flank the LR in the vicinity of the North Pole.

recognized by an increase in compressional wave velocity (from sonobouy modeling) that accompanies a transition into a series of high-amplitude reflectors that qualitatively resemble sediments deposited in shallow water environments [e.g., *Jokat*, 2005]. Along the crest of the LR, postrifting Cenozoic sediments have velocities <3 km/s, while velocities that exceed 4 km/s characterize the underlying Mesozoic sediments [*Jokat*, 2005]. However, the only ground-truthed seismic interpretation comes from core-seismic integration of the ACEX record with seismic lines AWI-91090 and 91091 (Figure 3) [*Jakobsson et al.*, 2006, 2007; *Backman et al.*, 2008]. On these lines, the increase in compressional wave velocity is abrupt and steps from 2.2 to >4.0 km/s across the rifting unconformity [*Jokat et al.*, 1995] (Figure 2). On the Makarov Basin flank, the Mesozoic sediments form a prograding sequence characteristic of deposition on a continental slope and attest to the shallow water setting of the LR prior to rifting from the Barents-Kara shelf [*Jokat et al.*, 1992; *Jokat*, 2005]. The intersection of these sequences with the basal reflector defining the rifting unconformity at the ACEX site [*Jakobsson et al.*, 2006] clearly supports this interpretation.

[9] Prior to ACEX, an integrated seismic interpretation of the depositional sequences in the Amundsen basin and those on the crest of the LR (AWI-91090) was presented by *Jokat et al.* [1995]. This initial interpretation dated the base of the Cenozoic sediments on the LR at 49 Ma, and suggested that the rifting unconformity formed as the ridge subsided below sea level [*Jokat et al.*, 1995]. Results from ACEX show that sediments immediately above the rifting unconformity are the same age as the oldest identified magnetic anomalies in the Eurasian basin (~57 Ma) indicating that the unconformity is closely associated with early postrifting or synrift processes and that the crest of the LR was at or near sea level as oceanic crust was emplaced on the newly formed spreading axis. The identification of a terminal onlap event

in seismic unit AB4 of the Amundsen Basin was proposed to mark the transition from slope rise to pelagic sedimentation at 46 Ma, signifying the subsidence of the LR into deeper water depths [*Jokat et al.*, 1995]. The age for the terminal onlap sequence was estimated by the intersection of this prominent reflector with areomagnetically dated crust in the Amundsen Basin [*Jokat et al.*, 1995]. On a more recent crossing line of the Amundsen basin (AWI-20010300) [*Jokat and Micksch*, 2004], this same reflector onlaps onto slightly younger oceanic crust (~43 Ma), providing a younger estimate for the transition from ridge-influenced to pelagic sedimentation.

[10] The largest difference in the original seismic interpretation and drilling results from ACEX was the omission of the 26 Ma mid-Cenozoic hiatus. Although occurring along two stacked reversed-amplitude reflectors, it is a disconformity and therefore difficult to identify in the seismic data (Figure 2) [*Jakobsson et al.*, 2006]. Along lines AWI-91090 and 91091, there is no indication that the mid-Cenozoic unconformity becomes angular along the ridge crest. However, Cenozoic sediments on the flanks of the ridge are poorly resolved and obscured by mass wasting processes [*Kristoffersen et al.*, 2007]. Similarly, in the vicinity of the drill sites, there are no published crossing lines that image this unconformity as it progresses into shallower or deeper water depths. On regional lines that do traverse topographic highs (e.g., Oden 1996, ARK-XII/1; see Figure 3) seismic interpretations are complicated by erosion from iceberg scouring [*Kristoffersen et al.*, 2004].

[11] Detailed seismic data from between the North Pole and Greenland are sparse. Available data indicate variable thicknesses for sediments capping the crest of the ridge, with estimates ranging from >850 m for the ARLISS II crossing to <75 m along the LOREX drift path [*Weber and Sweeney*, 1985] (Figure 3). Thinner sediments are evidenced nearer the Greenland margin, where *Kristoffersen and Mikkelsen* [2006] report thicknesses of <50 ms (two-way travel time) where the ridge crest shallows to within 500 mbsl. Sediments on the slope of this topographically elevated region reveal an expanded onlapping sequence that reflects deposition on the flank of a subsiding margin [Unit D in *Kristoffersen and Mikkelsen*, 2006]. Although speculative, the base of this unit is assigned to the Cretaceous and the top to sometime in the Plio-Pleistocene [*Kristoffersen and Mikkelsen*, 2006], inferring that the crest of this shallow segment remained near sea level well into the Miocene.

[12] A change in both the structural makeup and nature of sedimentary cover south of ~85°N on the Siberian Margin side of the North Pole suggests a different tectonic and subsidence history for this segment of the LR [*Jokat*, 2005]. Here the ridge becomes more structurally complex, and breaks into a series of at least 3 major blocks that spread out over a width of 200 km [*Jokat*, 2005; *Cochran et al.*, 2006]. The intervening troughs are filled with sediments between 1.5 and 3 km thick [*Jokat*, 2005]. Sonobuoy data collected along seismic lines in this region indicate that the transition between Mesozoic and Cenozoic sediments is more gradual, suggesting that the Mesozoic sediments were not as heavily influenced by erosion as those underlying the ACEX drill sites at ~88°N [*Jokat*, 2005]. The more segmented ridge and potentially less eroded Mesozoic sediments may be attributed to a higher degree of crustal extension in the Mesozoic, leaving these portions of the LR in deeper water depths during the prerift and synrift development of the Eurasian Basin.

[13] Toward the Siberian margin, there is no indication of onlapping sequences in what are interpreted to be postrifting Cenozoic sediments. In contrast, they are generally flat-lying, uninterrupted by recognized faults, and tend to follow the contours of the basement relief [e.g., *Jokat*, 2005; *Langinen et al.*, 2006]. None of the lines display a prominent reflector that can be unambiguously identified as stratigraphically coeval with the mid-Cenozoic hiatus at the ACEX site. The most prominent features in the published lines are a reversed-amplitude reflector within the Cenozoic sediments that is attributed to the presence of a Bottom Simulating Reflector (related to methane hydrates), and the high-amplitude reflectors that mark the base of postrift Cenozoic sediments [*Jokat*, 2005].

[14] Although differences in sediment thickness could potentially be used to identify differential subsidence rates, cumulatively, there does not appear to be a direct correlation between the thickness of Cenozoic sediments capping the topographic highs, and modern water depths [*Jokat*, 2005], reflecting the complexity of processes that affect different regions of the LR. These complex processes include sediment supply [e.g., *Jokat*, 2005], current activity [e.g., *Blasco et al.*, 1979], iceberg scouring [e.g., *Polyak et al.*, 2001; *Kristoffersen et al.*, 2004] and subsidence history.

3. ACEX Drilling Results

[15] One of the most surprising findings from ACEX was the presence of a 26 Ma long hiatus separating middle Eocene (44.4 Ma) from early Miocene (18.2 Ma) sediments [*Backman et al.*, 2008]. This hiatus separates two distinct modes of sedimentation. Paleogene sediments account for about 200 m of the recovered sequence and are rich in organic-walled and siliceous microfossils [*Backman et al.*, 2008; *Expedition 302 Scientists*, 2006]. These sediments transition from older siliclastic claystones having a total organic carbon content (TOC) of ~1%, to younger finely laminated biosiliceous-rich silty clays with TOC values between 2 and 3% [*Expedition 302 Scientists*, 2006; *Moran et al.*, 2006; *Stein et al.*, 2006]. They describe sediment deposition in predominantly euxinic and anoxic bottom water settings [*Stein et al.*, 2006]. Above the hiatus, Neogene sediments are fossil-poor silty clays interspersed with frequent sand lenses and drop stones [*Expedition 302 Scientists*, 2006] that describe an environment dominated by ice [*Moran et al.*, 2006].

[16] The lack of preserved benthic foraminferal assemblages make it difficult to construct a detailed subsidence pattern for the LR; however, paleodepth estimates from fossilized remains of surface dwelling assemblages suggest a shallow water, continental shelf setting for most of the Paleogene [*Expedition 302 Scientists*, 2006; *Moran et al.*, 2006] (Figure 2). These assemblages are dominated by diatoms composed entirely of neritic (shallow water) marine species [*Stickley et al.*, 2008]. A strong freshwater influence

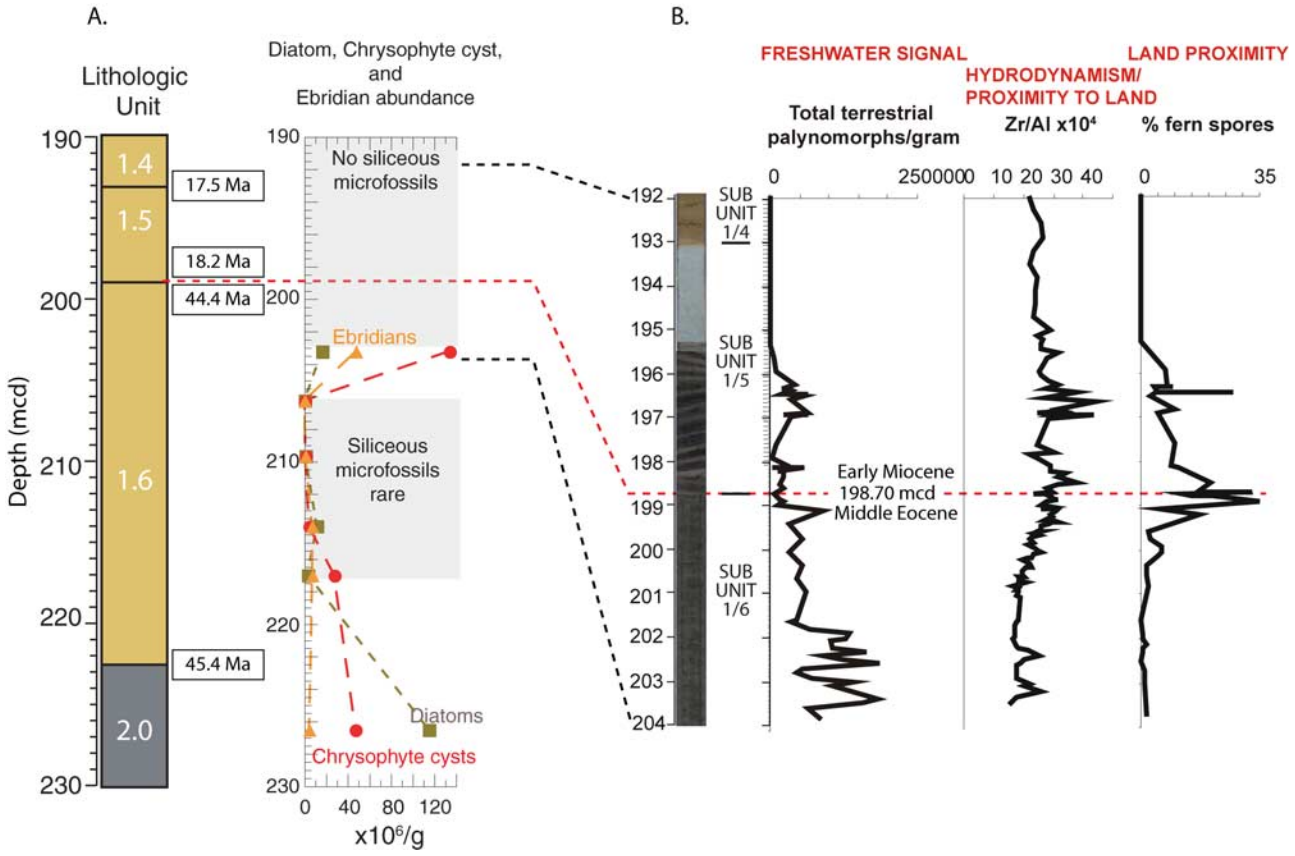

Figure 4. Micropaleontological and geochemical records from sediments bounding the hiatus. (a) Absolute abundances of diatoms, ebridians, and chrysophyte cysts, interpreted to be of shallow marine, brackish/shallow marine, and freshwater environments, respectively. Relative abundances of diatoms and chrysophytes in the upper part of the biosiliceous interval indicate decreasing salinities [*Stickley et al.*, 2008]. (b) Detailed summary diagram indicating the major paleoenvironmental changes across the hiatus as gathered from the multiproxy approach applied by *Sangiorgi et al.* [2008]. Lithostratigraphic column and image of core section containing the mid-Cenozoic hiatus (red line) prior to the start of cross-banded sediments.

is evident from the presence of chrysophyte algal cysts, brackish-to-freshwater organic-walled dinoflagellate cyst (dinocyst) assemblages and terrestrial palynomorphs (pollen and spores) as well as ebridians (siliceous-walled plankton that live in brackish waters) associated with mostly neritic environments [*Expedition 302 Scientists*, 2006]. Together these assemblages describe a shallow water setting with a fresh to brackish surface water lens that persisted throughout the Paleogene [*Expedition 302 Scientists*, 2006; *Brinkhuis et al.*, 2006].

[17] Changes in the microfossil assemblages in sediments leading up to the major Cenozoic hiatus record an increase in the abundance of freshwater tolerant species (Figure 4a). Small ebridians and chrysophyte cysts are the dominant siliceous microfossils while the diatom assemblage becomes nearly monospecific (Figure 4a). Palynological analyses reveal a growing terrestrial signal (Figure 4b), independently supported by geochemical analysis of preserved organic matter [*Stein et al.*, 2006], occurring with relatively well-preserved low-salinity dinocysts. A similar dominance of terrestrial over marine palynomorphs also occurred in the ACEX record around the Paleocene-Eocene thermal maximum (PETM) at 55 Ma, when inner neritic (<100 m) paleowater depths for the crest of the LR are constrained by benthic agglutinated foram assemblages [*Expedition 302 Scientists*, 2006; *Sluijs et al.*, 2006]. Perhaps more dramatically, the sudden appearance of fern spores immediately surrounding the hiatus suggests unroofing of the ridge crest in very close proximity to the drilling sites. Thus the increased abundance of freshwater tolerant species and terrestrially sourced material is strongly linked to a drop in relative sea level that brought the LR into the fresh to brackish surface water lens that existed throughout the Paleogene, exposing proximal topographic highs.

[18] Above the hiatus, the shift from biosilica-rich shallow marine deposits to fossil-poor glaciomarine silty clays [*Expedition 302 Scientists*, 2006; *Moran et al.*, 2006] involves a transitional phase characterized by a striking 5.76 m interval of cross-banded sediments. At the base of the cross-banded interval, a quasi-monospecific dinocyst

assemblage co-occurs with terrestrial and freshwater aquatic palynomorphs [*Sangiorgi et al.*, 2008]. This assemblage again reflects a restricted, shallow, brackish water setting, similar to that described in sediments before the hiatus [*Sangiorgi et al.*, 2008]. Further lines of evidence support a shallow water setting for sediments above the hiatus. The centimeter-scale tilted gray-to-black crosscutting couplets suggest deposition in either a nearshore or high-energy shallow water environment, an observation supported by the relative enrichment of the heavy mineral zircon (see Zr/Al ratio in Figure 4), in sediments surrounding the hiatus [*Sangiorgi et al.*, 2008]. Palynological assemblages also reveal reworked dinocysts from the Cretaceous, Paleocene, Eocene and even Oligocene, occurring within the cross-banded sequence [*Expedition 302 Scientists*, 2006], supporting the assertion that local unroofing and erosion of the ridge crest occurred during this time.

[19] On the basis of the analysis of the recovered material, a shallow water setting for the LR is inferred from the middle Eocene until the early Miocene. The duration of this episode is important for two reasons: (1) It means that the shoaling of the LR cannot be explained by a single decrease in global sea level, such as the 70 m estimated drop associated with Eocene–Oligocene ice growth on Antarctica at 34 Ma [*Peckar et al.*, 2002] and (2) the opening of the Fram Strait and the ventilation of the Arctic Ocean in the early Miocene, although invoked to explain the transition out of organic-rich deposition on the LR [*Jakobsson et al.*, 2007], cannot explain the shallow water setting that existed both prior to and after the hiatus.

4. Subsidence Models

[20] By using a benthic agglutinated foraminiferal assemblage indicating neritic conditions at 54 Ma, and the modern unloaded depth to the seafloor (1000 mbsl) at the ACEX sites, a model was proposed for the LR that assumed oceanic-type thermal cooling controlled the postrifting subsidence [*Moore and the Expedition Scientists*, 2006]. Conceptually, this model is justified by (1) the modern depth of the LR is predicted by isostatic arguments [*Weber and Sweeney*, 1990] and (2) thermal cooling controls both the postrifting subsidence of passive margins, and the subsidence of newly formed oceanic crust.

[21] Further corroboration that the LR is in isostatic equilibrium is achieved by comparing the unloaded depths of the LR and the oceanic crust in the Amundsen Basin. In the vicinity of the North Pole, the seafloor above the oldest oceanic crust in the Amundsen Basin is found at 4400 mbsl, with 2100 m of Cenozoic sedimentary cover [*Jokat and Micksch*, 2004]. Assuming an average sediment density of 1900 kg/m^3, and a mantle density of 3300 kg/m^3, the unloaded depth to basement (equation (1)) is 5208 mbsl.

$$D_{\text{Sedimentunloaded}} = D_{\text{current}} - S\left(\frac{\rho_m - \rho_s}{\rho_m - \rho_m}\right) \tag{1}$$

where S is the sediment thickness (m), ρ_m is the mantle density (kg/m^3), ρ_w is the density of seawater (1024 kg/m^3) and ρ_s is the average density of the overlying sediments (kg/m^3). Similarly, with an initial depth of 1250 mbsl, a sediment thickness of 420 m, and an average sediment density of 1800 kg/m^3, the unloaded depth to the Mesozoic basement at the ACEX drill sites is 973 mbsl.

[22] The difference between the unloaded ridge crest and adjoining oceanic crust is 4235 m. This agrees well with the predicted offset of 4262 m (equation (2)) between the 7 km thick section of oceanic crust (h_{oc}) adjoining the LR in the Amundsen basin [*Weigelt and Jokat*, 2001] with an average density of 2900 kg/m^3 (ρ_{oc}), and a 25 km thick piece of continental crust (h_c), with a density of 2800 kg/m^3 (ρ_c) using a mantle density (ρ_m) of 3300 kg/m^3 and seawater density (ρ_w) of 1024 kg/m^3.

$$\text{Elevation} = \frac{\rho_m - \rho_c^*}{\rho_m - \rho_w} h_c - \frac{\rho_m - \rho_{oc}^*}{\rho_m - \rho_w} h_{oc} \tag{2}$$

Employing a larger estimate of the modern crustal thickness for the LR (i.e., 28 km) results in an offset of 4920 m, suggesting that the ridge is deeper than isostatic predictions, but should be below sea level today.

[24] The classic model for the subsidence of passive margins describes two main components. The first is controlled by isostatic adjustments to mechanical thinning of the crust during stretching, while conductive thermal cooling controls the second stage as rifted margins drift from the newly formed spreading axis [*McKenzie*, 1978]. The amount of synrift tectonic subsidence and the amount and rate of postrifting thermal subsidence are controlled by the degree of lithospheric stretching, defined as the stretching factor (β):

$$\beta = \frac{h_{cc1}}{h_{cc2}} \tag{3}$$

where h_{cc1} is the initial thickness (or width) of the continental crust and h_{cc2} is the stretched thickness (or width) of the continental crust.

[25] McKenzie's model is based on a set of simplifying assumptions stipulating that airy isostasy is maintained throughout the rifts evolution and that the stretching of the crust and lithosphere occurs both instantaneously and is uniform with depth. Furthermore, radiogenic heat production in the crust is ignored and vertical conductive cooling controls dissipation of heat from a constant basal lithospheric temperature [*Allen and Allen*, 2005]. The tectonic subsidence is thereby modeled as occurring instantaneously, and is dependent upon the initial crustal thickness and the amount of stretching. The initial tectonic subsidence (S_t) is calculated by

$$S_t = \frac{Y_l\left\{(\rho_m^* - \rho_C^*)\frac{Y_c}{Y_L}\left(1 - \alpha_v \frac{T_m Y_c}{2Y_L}\right) - \frac{\alpha_v T_m \rho_m^*}{2}\right\}(1 - 1/\beta)}{\rho_m^*(1 - \alpha_v T_m) - \rho_w} \tag{4}$$

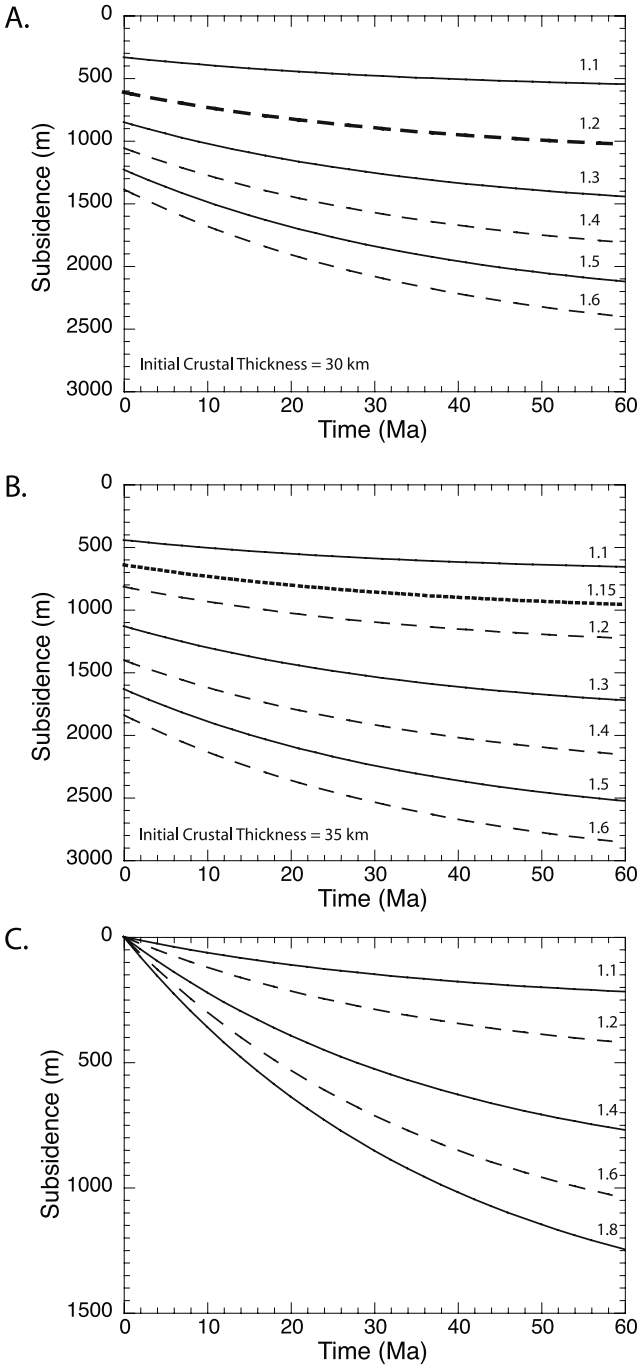

Figure 5. Total subsidence as predicted by *McKenzie*'s [1978] uniform extension model using different stretching factors with (a) an initial crustal thickness of 30 km and (b) an initial crustal thickness of 35 km. (c) Thermal subsidence predictions when initial conditions are set to depth equal to 0 mbsf when T = 0 Ma.

where β is the stretching factor, α_v is the thermal expansion coefficient of the crust and mantle, ρ_m* is the mantle density at 0°C, ρ_c* is the crustal density at 0°C, ρ_w is the density of seawater, T_m is the asthenospheric temperature, Y_L the initial thickness of the lithosphere and Y_c the initial crustal thickness (see Table 1).

[26] Subsidence associated with the postrift thermal cooling is a function of both the stretching factor and time:

$$S_{th}(t) = E_o \frac{\beta}{\pi} \sin\left(\frac{\pi}{\beta}\right)\left(1 - e^{-t/\tau}\right) \quad (5)$$

with $S_{th}(t)$ the amount of thermal subsidence in meters at time (t), and E_o defined by:

$$E_o = 4 y_L p_m \alpha_v T_m / \pi^2 (p_m - p_w) \quad (6)$$

where α_v is the thermal expansion coefficient (°C$-^1$) for the lithosphere.

[27] As with other rifted margins, maximum stretching of the continental crust occurs at the continent-ocean transition in the Amundsen Basin, where β approaches infinity. Toward the center of the highstanding portions of the LR, significantly less stretching occurs. In applying the McKenzie model, we assume that seismically imaged faulting [*Jokat et al.*, 1992] beneath the Cenozoic sediments at the ACEX sites are attributed to stretching that occurred during the early Cenozoic rifting of the LR from the Barents-Kara shelf, and address the implications of zero crustal stretching on the highstanding portions of the LR below.

[28] Although there is no direct evidence for the prestretching thickness of the crust beneath the LR, modern crustal thicknesses range between 30–35 km for the outer part of the Barents shelf between Svalbard and Franz-Josef Land [*Ritzmann et al.*, 2007]. Taking these latter estimates as the minimal initial crustal thickness (h_{cc1}) and the reported range of current crustal thicknesses for the LR of 25–28 km (h_{cc2}), the expected stretching factor falls between 1.1 and 1.4.

[29] The total subsidence predicted by *McKenzie*'s [1978] model for these stretching factors is presented in Figure 5 and is determined by summing the expected tectonic subsidence and the thermal subsidence. A stretching factor between 1.15 and 1.2 provides the best fit for generating 1000 m of total subsidence since the end of rifting ~57 Ma. A β of 1.15 corresponds to an initial crustal thickness of 35 km and results in a modern thickness of 30.4 km, while a

Table 1. Parameters Used in Subsidence Modeling

Parameter	Definition	Units	Value
T_m	temperature at base of lithosphere	°C	1330
T_0	temperature at seafloor	°C	0
Y_L	thickness of lithosphere	Km	110
K	thermal conductivity of lithosphere	W/mK	3.3
κ	thermal diffusivity of lithosphere	M^2/Ma	3.15×10^7
T	time	Ma	57
τ	thermal time constant of lithosphere	Ma	50.25
p_m	density of mantle at 0°C	kg/m^3	3330
α_v	coefficient of thermal expansion for crust and mantle	1/°C	3.28×10^{-5}
p_w	density of seawater	kg/m^3	1024

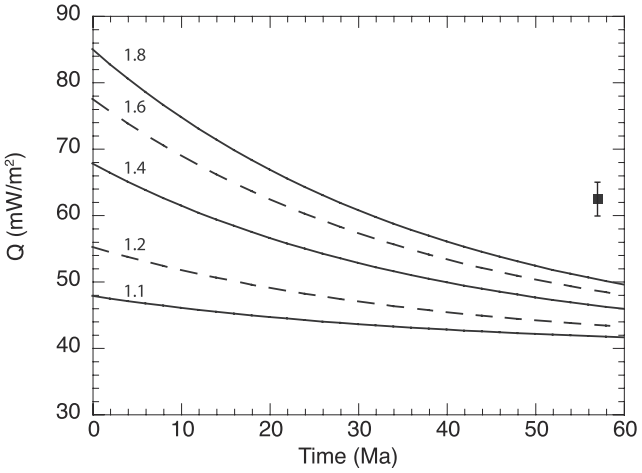

Figure 6. Surface heat flow as predicted by *McKenzie*'s [1978] uniform extension model using different stretching factors. The black box indicates the range of reported heat flow values from the LOREX expedition [*Langseth et al.*, 1990].

β of 1.2 corresponds to an initial crustal thickness of 30 km and results in a modern thickness of 25 km. Although reproducing the total amount of observed subsidence with moderate stretching factors, the results are clearly at odds with drilling results from ACEX, where at the start of seafloor spreading, the crest of the LR was in an inner neritic (<100 mbsl) setting. Thus, if the modern depth below sea level of the LR is explained by a 13–16% reduction in the lithospheric thickness that accompanied rifting from the Barents-Kara shelf, then a possible scenario is that the crest of the LR was at or near sea level following the Mesozoic opening of the Eurasian Basin. Initial subsidence associated with the thinning of the crust was offset by doming above the incipient rift zone or flank uplift. Erosion during synrift exposure accounts for the peneplained surface separating Cenozoic and Mesozoic sediments on this segment of the LR [*Jokat et al.*, 1992, 1995; *Jokat*, 2005; *Jakobsson et al.*, 2006]. By 57 Ma, the crest of the ridge had returned to sea level, but the subsequent subsidence associated with crustal thinning and thermal equilibration was impeded until the early Miocene.

[30] An alternative approach to the 1-D modeling attributes the 1000 m of subsidence since 57 Ma to conductive thermal cooling. This approach requires that most of the synrift tectonic subsidence (faulting associated with stretching) ended by 80 Ma, when the drilling results place the depth of the ridge crest in an inner neritic setting. The more protracted nature of the rifting event transfers more of the total subsidence to the synrift stage [e.g., *Cochran*, 1983] increasing the already high stretching factor (β>1.4) required to account for the observed subsidence (Figure 5). A stretching factor of this magnitude is unsupported by the limited extent of seismically imaged faulting on this portion of the LR. The high stretching factor also implies substantially larger initial crustal thicknesses (>40 km) and requires synrift tectonic subsidence that exceeds 1500 m, placing the LR and conjugate Barents-Kara shelf at more than 1.5 km above sea level prior to the start of rifting.

[31] Admittedly, there is considerable uncertainty in stretching values derived from 1-D subsidence analyses in which flexural influences, introduced by differential sediment loading and crustal extension are ignored. For example, in the East Shetland Basin of the northern North Sea, 1-D models produce estimates of β that are 3 times higher than those produced by 2-D models that incorporate a flexural component to the subsidence analysis [*Roberts et al.*, 1998]. Similarly, depth-dependent stretching, where more stretching is localized in the ductile lower crust and upper mantle, can result in whole lithospheric stretching factors that exceed those inferred from analyses of upper crustal faulting [*Kusznir et al.*, 2004; *Davis and Kusznir*, 2004].

[32] In reverse modeling exercises, an additional constraint on the magnitude of the whole-lithosphere stretching factor is derived from heat flow data that can be directly compared with predictions from *McKenzie*'s [1978] model (Figure 6). For the LR, published heat flow measurements collected during LOREX fall between 60–65 mW/m^2 [*Sweeney et al.*, 1982; *Langseth et al.*, 1990] but no additional information is given pertaining to the location, thermal gradients, or conductivity profiles used to derive these estimates. In situ temperature measurements during ACEX produced scattered results [*Expedition 302 Scientists*, 2006]. Coupled with uncertainties in the radiogenic heat production of the crustal layers (required to bring the reported heat flow into the range predicted by stretching factors of < 10), the existing data from the LR does not help resolve the relatively small differences in surface heat flow associated with changes in β after ~50 Ma (Figure 6).

[33] Certainly, the total subsidence analysis employing stretching factors of 1.1–1.2 are more consistent with seismic observations on the degree of faulting, and best explain the current depth to the crest of the LR. However, despite the stretching factor applied, the 1-D modeling clearly illustrates that a shallow water setting in the early Miocene requires a prolonged period of stalled subsidence, a phase of postrift uplift, or extraordinarily large sea level variations (Figure 7).

5. Mechanisms to Influence the Subsidence of the LR

[34] The ACEX drilling results clearly show that the LR did not follow a smooth thermally controlled postrifting subsidence pattern. However, many of the passive margins that border the North Atlantic and Arctic Ocean have undergone episodes of uplift [*Eyles*, 1996; *Rohrman and van der Beek*, 1996; *Doré et al.*, 2002; *Tsikalas et al.*, 2005; *Japsen and Chalmers*, 2000; *Japsen et al.*, 2006] and accelerated subsidence [*Cloetingh et al.*, 1985, 1990; *Kooi et al.*, 1991; *Cloetingh and Kooi*, 1992] during the Cenozoic. There are a range of factors influencing the postrifting subsidence of passive margins [e.g., *Ziegler and Cloetingh*, 2004] which include the mode and evolution of continental extension [*Buck*, 1991], variations in asthenospheric tem-

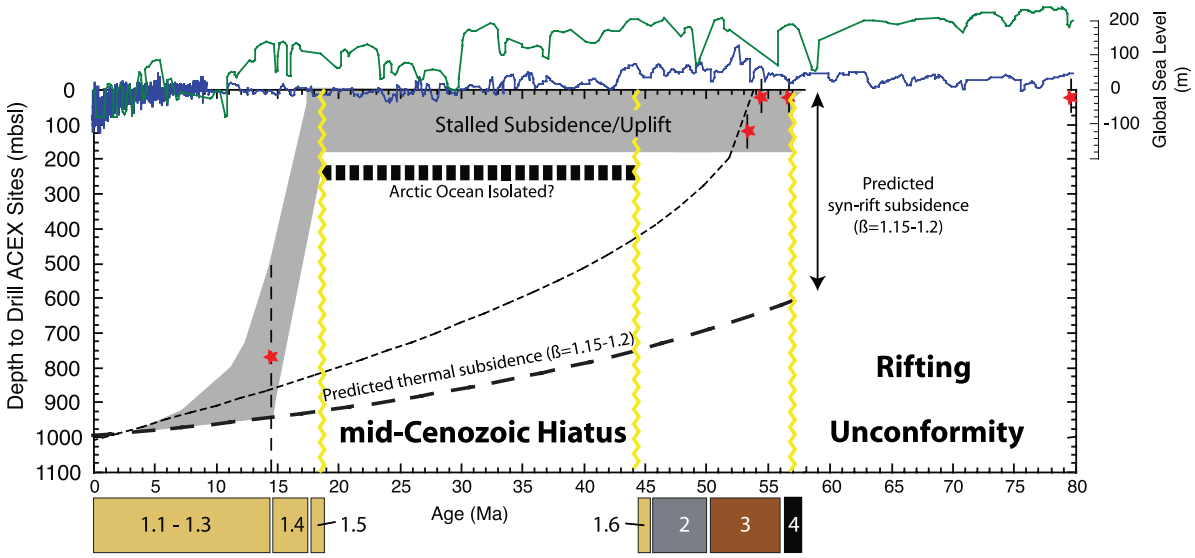

Figure 7. Subsidence models for the Lomonosov Ridge. Previously published subsidence model of *Moore and the Expedition 302 Scientists* [2006] (short-dash line) and a subsidence curve generated using the *McKenzie* [1978] model (long-dash line) employing a stretching factor of 1.15. Boundaries and ages of lithostratigraphic units are from *Backman et al.* [2008]. Paleodepth estimates from subsidence models contrast with micropaleontological estimates from surface assemblages (shaded grey). Benthic agglutinated foram constraints on the paleowater depth are illustrated by a star with the associated depth range indicated by grey bar [*Expedition 302 Scientists*, 2006]. Variations in global sea level curves are from *Haq et al.* [1987] (green) and *Miller et al.* [2007] (blue).

peratures and magmatic production at the spreading axis, postrift lateral heat conduction [*Steckler*, 1985], flexural uplift arising from variable lithospheric thicknesses or sediment loads [*Watts*, 2001], synrift and postrift metamorphic mineral phase transitions [*Kaus et al.*, 2005] and responses to changes in the in-plane stress fields around tectonic plates [*Cloetingh et al.*, 1985, 1999].

[35] A prolonged postrifting shallow water setting for the LR is in keeping with observations made on modern analogues such as the Baja Peninsula bordering the Gulf of California, and the island of Socotra in the eastern Gulf of Aden. In both instances, fragments of continental crust remain above sea level 7–8 Ma [*Kier et al.*, 2001] and 18 Ma [*Leroy et al.*, 2004] after the emplacement of oceanic crust along a rift zone. One possible explanation for this setting is that the portion of the LR underlying the drilling sites was not extended during rifting from the Barents-Kara shelf. This is analogous to assuming that the highstanding portion of the LR is a rift flank, found landward of the hinge zone, and the underlying faults cutting Mesozoic sediments are inherited from the opening of the Canada Basin.

[36] Synrift and postrift flank uplift is a common phenomenon often attributed to lithospheric flexure [*Weissel and Karner*, 1989] and isostatic adjustments to depth-dependent necking [*Braun and Beaumont*, 1989] but is also linked to deep crustal flow [*Hopper and Buck*, 1996] and thermal convection [*Keen*, 1985; *Buck*, 1986]. The magnitude and duration of thermally induced vertical movements was recently demonstrated using a 2-D finite element model of the thermal evolution of rifted margins [*Leroy et al.*, 2008]. Their results showed that unstretched lithosphere flanking rift zones undergoes a phase of postbreakup thermal thinning that results in uplift, and is followed by thermal thickening causing subsidence. The transient modeled uplifts last ~80 Ma and at nonvolcanic passive margins translate into vertical motions that are <150 m. Modeled as an unstretched rift flank, the outstanding question becomes why the LR subsided at all in the early Miocene. Both the rate and magnitude of subsidence in the ACEX record are larger, and occur earlier, than the thermal model of *Leroy et al.* [2008] would predict. We argue that the modern depth of the LR is related to lithospheric stretching accompanying the opening of the Eurasian Basin, and thus an alternate mechanism is required to explain the delayed subsidence.

[37] Linking results from kinematic plate models, and structural observations on the margins of the Arctic Ocean, a prolonged phase of basin-wide compression is evident from 56 Ma to 20 Ma. The documented compression occurred in two stages (Figure 8). The first is associated with the independent movement of the Greenland microplate, which, between 56 Ma and 33 Ma, was acting as a triangular indenter and impinging on the growing Eurasian Basin [*Lawver et al.*, 2002; *Brozena et al.*, 2003]. Onshore, this compression is apparent in the orogenies of the Ellesmere and Svalbard Islands and more recently mapped in the Eurasian Basin where ~200 km of crustal shortening is linked with broad east-west trending gravity lows that flank the Morris Jesup Rise and Yermak plateau [*Brozena et al.*, 2003]. The documented crustal shortening is predicted by plate kinematic reconstructions and ends at C13 [*Brozena et al.*, 2003] during a period of circumarctic plate reorganiza-

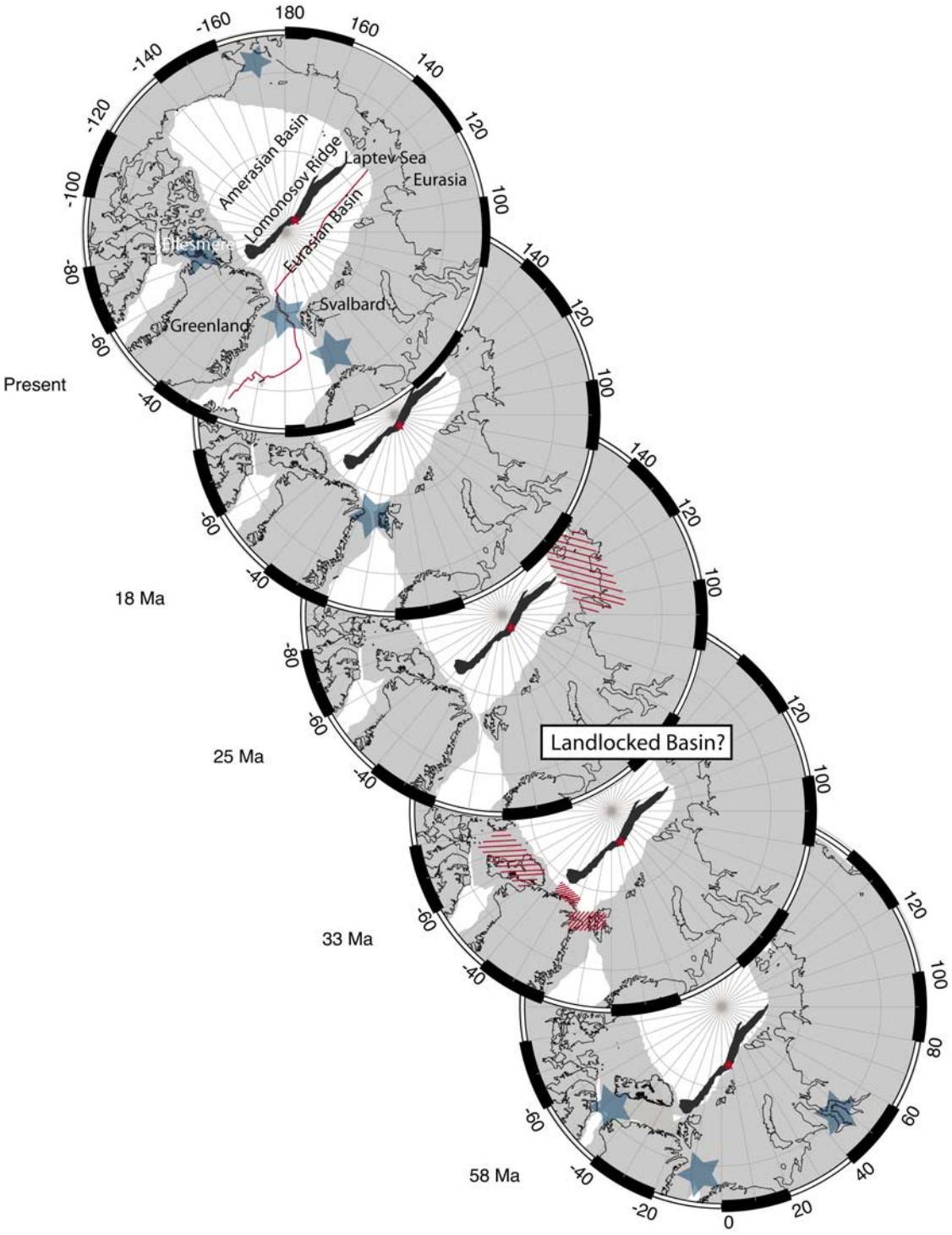

Figure 8. Snapshots of the Cenozoic tectonic evolution of the Arctic Ocean. Plate reconstructions are from the Ocean Drilling Stratigraphic Network tools, available online at www.odsn.de. Plate boundaries are shaded gray and illustrated with modern shorelines. Hatching denotes areas of documented compressional tectonic deformation (see text). Stars indicate connections to the world oceans.

tion, when Greenland first began to move with the North American plate.

[38] The plate reorganization at C13 is associated with the migration of the Euler pole for the North American and Eurasian plates, which between C13 and C6 (19–24 Ma) migrated toward the Lena Delta on the edge of the Laptev Sea continental margin [*Drachev et al.*, 2003; *Glebovsky et al.*, 2006]. As a response to the change in the position of the

Euler pole, maximum spreading rates on the central Gakkel Ridge dropped from 20 to 6 mm/a, while at the transition to the Laptev shelf the rates decreased from 12.5 to <1 mm/a [*Vogt et al.*, 1979; *Drachev et al.*, 2003]. On the Laptev and Siberian shelves, onshore sequences show a prominent hiatus beginning at C13 [*Drachev et al.*, 1998]. This regional unconformity is associated with tectonic compression/transpression that persisted until C6, evidence of which is preserved in a series of thrusts and reverse faults mapped on the New Siberian Islands and in the northern Verkhoyansk Range (Figure 8) [*Drachev et al.*, 1998]. Plate tectonic reconstructions thus suggest that the Eurasian Basin was subjected to far-field compressional forces from its inception until the early Miocene, overlapping with the inferred period of stalled/inverted subsidence seen in the ACEX record.

[39] Observations on the subsidence patterns preserved in wells from the central North Sea, west Greenland, Labrador, Scotian Shelf and the western mid-Atlantic margin all display accelerated basin-center subsidence and margin uplift in response to increased far-field compression [*Cloetingh et al.*, 1985, 1990]. Early modeling showed that in-plane stresses, with magnitudes that approximate ridge push forces (5×10^{11} N/m^2) [*van Balen et al.*, 1989], accentuate ltihospheric and crustal deflections inherited during rifting [*Cloetingh et al.*, 1985; *Karner*, 1986]. More recent efforts, incorporating a multilayered continental lithosphere, further illustrate that thicker crustal sections found landward of the rift become uplifted when compressional stress increases [*van Balen et al.*, 1998]. This flexural response to in-plane stress has been used to account for differential subsidence patterns across the North Sea Basin [*Kooi and Cloetingh*, 1989; *van Wees and Cloetingh*, 1996], the Beaufort-Mackenzie Basin [*Tang and Lerche*, 1992] and the Barents Sea [*Reemst et al.*, 1994]. The documented compression of the Eurasian Basin thus provides a mechanism for stalling the subsidence of the LR, and possibly inducing some postrifting uplift.

[40] One obstacle to invoking compression to explain the stalled subsidence/uplift of the LR is the lack of evidence for faulting in the available inventory of seismically imaged Cenozoic sediments (Figures 2 and 3). In the flexural subsidence model presented by *van Balen et al.* [1998], margin uplifts are mainly associated with subcrustal stress-induced deflections, and not necessarily manifest in the reactivation of surface faults. However, the broad domal uplift of the entire ridge is an unlikely response, so some degree of differential block uplift or faulting is required to stall or especially invert the postrifting subsidence. Although extensive differential block uplift was suggested for the LR in the mid-Cenozoic [*Kim et al.*, 2001; *Butensko and Poselov*, 2006], these interpretations were based on a mid-Cenozoic date for the rifting unconformity identified in the ACEX record. On the basis of the core-seismic integration at ACEX [*Jakobsson et al.*, 2006; *Backman et al.*, 2008], the arguments presented in these papers support the assertion that substantial along-strike faulting accompanied the initial rifting of the LR from the Barents-Kara shelf.

[41] Flexural uplifts, generated by compression, may have operated in unison with thermal and/or mineral phase transitions. For instance, the LR is flanked by gravity lows and disrupted magnetic anomalies that appear strongest in the circumpolar regions of the ridge (Figure 3) [*Vogt et al.*, 1979; *Brozena et al.*, 2003; *Cochran et al.*, 2006]. These characteristics, attributed to serpentinization at the Iberian margin [*Whitmarsh et al.*, 1993; *Whitmarsh and Miles*, 1995; *Whitmarsh et al.*, 2001], may also indicate serpentinization of mantle peridotite underlying parts of the LR. Uplift, induced by transverse compression, might have been sustained by serpentinization, because of the associated mechanical weakening and volume expansion [*Skelton and Jakobsson*, 2007]. However, the contemporary presence of the gravity lows suggests that large-scale deserpentinization has not occurred, and thus cannot be invoked to explain the rapid early Miocene subsidence.

[42] The more complete transition into what are interpreted to be Mesozoic sediments on the Siberian Margin side of the LR [*Jokat*, 2005], and the lack of any well developed reflector in the middle of the Cenozoic sediments on these profiles, does suggest that unroofing and erosion may be confined to segments of the LR that lie north of 84°–85°N of the Siberian margin. Unless compression was localized near the circumpolar bend in the LR, the same subsidence pattern is likely closer to the Siberian margin, but deeper initial water depths prevented unroofing of these segments in the mid-Cenozoic. Although there is less seismic coverage on the Greenland margin side, the generally monolithic structure of the ridge between Greenland and the North Pole, coupled with the pronounced onlapping sequences on the slope of the Greenland margin flank [*Kristoffersen and Mikkelsen*, 2006], would predict that this segment shares the same tectonic, subsidence and depositional history as the region visited during ACEX.

6. Sea Level Variations and Paleoceanographic Implications

[43] The preserved sequence of Paleogene sediments at ACEX, which describe a progression from euxinic to finely laminated anoxic bottom water conditions [*Stein et al.*, 2006], was initially used to support the assertion that the LR had subsided to 350 mbsl, beyond the modern depth of eddy mixing (~200 m) [*Aagaard and Carmack*, 1989; *Moore and the Expedition 302 Scientists*, 2006]. Ultimately, the mixed surface layer of the Eocene Arctic Ocean would be related to the strength and position of the pycnocline. Throughout the Eocene a freshwater surface layer coexists with reducing conditions on the seafloor, indicating that the crest of the ridge was below the pycnocline. The only controls on the depth of the pycnocline come from biomarkers in sediments from around the PETM [*Sluijs et al.*, 2006, 2008], which suggest anoxia in the photic zone. Thus, a very shallow and strong pycnocline could have been a persistent feature of the Arctic until the ventilation of the basin occurred with the opening of the Fram Strait [*Jakobsson et al.*, 2007], requiring only minimal subsidence of the ridge crest prior to the Miocene. There is certainly enough variability within and between global eustatic estimates to account for changes in the composition of the Paleogene surface assemblages in the ACEX record without

invoking a period of uplift (Figure 7). Within this setting, the coincidence between the shoaling of the LR captured in the micropaleontological data immediately before the hiatus, and the end of a global sea level highstand witnessed through the Paleogene in the record of *Miller et al.* [2007] (Figure 7), appear linked.

[44] Although a seemingly shallow water setting at the ACEX drill sites persisted until the early Miocene, reconstructing precise paleowater depth estimates is complicated by both the lack of benthic assemblages in the ACEX record and the poorly constrained variation in basin-wide sea level. Following the closure of the Turgay strait by the middle Eocene [*Akhmets'ev and Beniamovski*, 2006; *Radionova and Khokhlova*, 2000] shallow seaways on the eastern and western margins of Greenland were the only links to the global oceans. With the northward motion of Greenland and the development of the Tertiary Ellesmere and Svalbard orogenies, the persistence of these shallow connections through the mid-Cenozoic remains rather speculative. Studies on benthic agglutinated foram assemblages from the Mackenzie delta describe a low diversity and entirely endemic assemblage persisting throughout the Eocene [*Young and McNeil*, 1984] an observation attributed to the largely isolated nature of the basin. However, following a large hiatus, assemblages assigned to the Oligocene show affinities with North Atlantic and European specimens, and are used to argue for partial connections to the world oceans [*McNeil*, 1990].

[45] After the tectonic closure of gateways in the Eocene, it is certainly possible that until the opening of the Fram Strait in the early Miocene [*Jakobsson et al.*, 2007] the Arctic Ocean may have remained predominantly isolated, and susceptible to large climatically driven variations in sea level. Pan-Arctic Eocene-Oligocene age unconformities reported in outcropping sediments on the east Siberian and Laptev shelves [*Drachev et al.*, 1998], the Barents-Kara shelf [*Zarkhidze*, 1992] and south western Barents Sea [*Worsley*, 2006], as well as in exploration wells from the Beaufort Mackenzie basin [*Dietrich et al.*, 1985], may record transgressive and regressive events that far exceed estimates from global eustatic records.

[46] The cross-banded sediments occurring above the hiatus are the remnants of depositional/erosional processes that persisted through the mid-Cenozoic while the crest of the LR remained at or near sea level. Agglutinated foram assemblages are present again in the ACEX sediments in lithologic subunit 1.4 (Figure 7), and thus require that subsidence of the LR began in the early Miocene. The end of the cross-banded sequences in subunit 1.5 could either be related to the start of a rapid early Miocene subsidence of the ridge and/or signify the end of large-scale sea level variations that accompanied the initial widening of the Fram Strait. Sea level changes occurring while the crest of the LR remained near to sea level also explain the occurrence of reworked Oligocene specimens and Miocene foram linings indicative of neritic to midbathyl depths [*Sangiorgi et al.*, 2008] that occur in the cross-banded sediments and are more difficult to account for if a single episode of uplift and subsidence was invoked.

[47] While additional constraints on the subsidence history for the segment of the LR visited during ACEX could be derived from crossing seismic lines that traverse proximal topographic highs; unraveling the effects of sea level variation from local tectonic processes is best achieved by correlating the ACEX record with seismic and coring data from other physiographic features in the Arctic Ocean.

7. Conclusions

[48] Here we have synthesized drilling results from ACEX with regional geophysical and plate tectonic observations to explain the occurrence of a 26 Ma mid-Cenozoic hiatus on the crest of the LR. The hiatus is shown to result from unroofing and erosion of the ridge crest, an observation that is at odds with predictions from tectonic subsidence models that attempt to explain the postrifting subsidence as a result of thermal cooling following stretching. A prolonged shallow water setting for the crest of the LR cannot be explained by global changes in sea level, unless tectonic processes affected the subsidence pattern of the LR and/or decoupled regional sea level from global eustatic estimates. The rapid onset of subsidence in the Miocene is synchronous with the end of compressional tectonics in the Eurasian basin and is the preferred mechanism to account for the anomalous subsidence pattern. More detailed subsidence modeling incorporating flexural effects and the related influence of far-field in-plane stresses is required to test this preferred hypothesis. These efforts would benefit from additional constraints on regional heat flow trends and the prerifting configuration of the LR and Barents-Kara shelf.

[49] **Acknowledgments.** Financial support was provided by the National Science Foundation (award 0623220), the U.S. Science Support Program of the Joint Oceanographic Institutions (JOI) Inc., the Swedish Research Council, and the Netherlands Organization for Scientific Research. This research was conducted with samples and data from the Integrated Ocean Drilling Program (IODP), an international marine research program dedicated to advancing scientific understanding of the Earth, the deep biosphere, climate change, and Earth processes by sampling and monitoring subseafloor environments. We thank the IODP European Science Operator (ESO) and the Swedish Polar Research Secretariat as well the ship fleet management, captains, and crews of the ships *Oden*, *Vidar Viking*, and *Sovetskiy Soyus*.

References

Aagaard, K., and E. C. Carmack (1989), The role of sea ice and other fresh water in the Arctic circulation, *J. Geophys. Res.*, *94*, 14,485–14,898.

Akhmets'ev, M. A., and V. N. Beniamovski (2006), The Paleocene and Eocene in the Russian part of west Eurasia, *Stratigr. Geol. Correl.*, *14*, 49–72.

Allen, P. A., and J. R. Allen (2005), *Basin Analysis: Principles and Applications*, 2nd ed., Blackwell, Oxford, U. K.

Backman, J., et al. (2008), Age model and core-seismic integration for the Cenozoic Arctic Coring Expedition sediments from the Lomonosov Ridge, *Paleoceanography*, doi:10.1029/2007PA001476, in press.

Blasco, S. M., B. D. Bornhold, and C. F. M. Lewis (1979), Preliminary results of surficial geology and geomorphology studies of the Lo-

monosov Ridge, central Arctic Basin, *Pap. Geol. Surv. Can.*, *79-1C*, 73–83.

Braun, J., and C. Beaumont (1989), A physical explanation of the relation between flank uplifts and the breakup unconformity at rifted continental margins, *Geology*, *17*, 760–764.

Brinkhuis, H., et al. (2006), Episodic fresh surface waters in the early Eocene Arctic Ocean, *Nature*, *441*, 606–609.

Brozena, J. M., V. A. Childers, L. A. Lawver, L. M. Gahagan, R. Forsberg, J. L. Fileide, and O. Eldholm (2003), New aerogeophysical study of the Eurasia Basin and Lomonosov Ridge: Implications for basin development, *Geology*, *31*, 825–828.

Buck, W. R. (1986), Small-scale convection induced by passive rifting: The cause for uplift of rift shoulders, *Earth Planet. Sci. Lett.*, *77*, 362–372.

Buck, W. R. (1991), Modes of continental lithospheric extension, *J. Geophys. Res.*, *96*, 20,161–20,178.

Butensko, V. V., and C. A. Poselov (2006), Regional paleotectonic interpretation of seismic data from the deep-water central Arctic, in *Proceedings of the Fourth International Conference on Arctic Margins: Dartmouth Nova Scotia*, *Canada*, *September 30–October 3*, *2003*, *OCS Study MMS 2006-003*, edited by R. Scott and D. Thurston, pp. 125–131, Dep. of the Inter., Anchorage, Alaska.

Cloetingh, S., and H. Kooi (1992), Tectonics and global change—Inferences from late Cenozoic subsidence and uplift patterns in the Atlantic/Mediterranean region, *Terra Nova*, *4*, 340–350.

Cloetingh, S., H. McQueen, and K. Lambeck (1985), On a tectonic mechanism for regional sea level variations, *Earth Planet. Sci. Lett.*, *75*, 157–166.

Cloetingh, S., F. M. Gradstein, H. Kooi, A. C. Grant, and M. Kaminski (1990), Plate reorganization: A cause of rapid late Neogene subsidence and sedimentation around the North Atlantic?, *J. Geol. Soc. London*, *147*, 495–506.

Cloetingh, S., E. Burov, and A. Poliakov (1999), Lithospheric folding: Primary response to compression? (from central Asia to Paris basin), *Tectonics*, *18*(6), 1064–1083.

Cochran, J. R. (1983), Effect of finite extension times on the development of sedimentary basins, *Earth Planet. Sci. Lett.*, *66*, 289–302.

Cochran, J. R., M. H. Edwards, and B. J. Coakley (2006), Morphology and structure of the Lomonosov Ridge, Arctic Ocean, *Geochem. Geophys. Geosyst.*, *7*, Q05019, doi:10.1029/2005GC001114.

Davis, M., and N. J. Kusznir (2004), Depth-dependent lithospheric stretching at rifted continental margins, in *Proceedings of NSF Rifted Margins Theoretical Institute*, edited by G. D. Karner, pp. 92–136, Columbia Univ. Press, New York.

Dietrich, J. R., J. Dixon, D. H. McNeil, D. J. McIntyre, L. R. Snowdon, and P. Brooks (1985), The geology, biostratigraphy, and organic geochemistry of the Natsek E-56 and Edlok N-56 wells, western Beaufort Sea, Arctic Canada, in *Current Research Pap. Geol. Surv. Can.*, 89-1A, 133–157.

Doré, A. G., J. A. Cartwright, M. S. Stoker, J. P. Turner, and N. White (2002), Exhumation of the North Atlantic margin: Introduction and background, in *Exhumation of the North Atlantic Margin: Timing*, *Mechanisms and Implications for Petroleum Exploration*, edited by A. G. Doré et al., *Geol. Soc. London, Spec. Publ.*, *196*, 1–12.

Drachev, S. S., L. A. Savostin, V. G. Groshev, and I. E. Bruni (1998), Structure and geology of the continental shelf of the Laptev Sea, eastern Russian Arctic, *Tectonophysics*, *298*, 357–393.

Drachev, S. S., N. Kaul, and V. N. Beliaev (2003), Eurasia spreading to Laptev shelf transition: Structural pattern and heat flow, *Geophys. J. Int.*, *152*, 688–698.

Expedition 302 Scientists (2006), Sites M0001–M0004, in *Arctic Coring Expedition* (*ACEX*), *Proc. Integr. Ocean Drill. Program*, *302*, doi:10.2204/iodp.proc.302.104.2006.

Eyles, N. (1996), Passive margin uplift around the North Atlantic region and its role in Northern Hemisphere late Cenozoic glaciations, *Geology*, *24*, 103–106.

Forsyth, D. A., and J. A. Mair (1984), Crustal structure of the Lomonosov Ridge and the Fram and Makarov basins near the North Pole, *J. Geophys. Res.*, *89*, 473–481.

Fütterer, D. K. (1992), ARCTIC '91: The expedition ARK VIII/3 of RV *Polarstern* in 1991, *Ber. Polarforsch.*, *107*, 1–267.

Glebovsky, V. Y., L. C. Kovacs, S. P. Maschenkov, and J. M. Brozena (2000), Joint compilation of Russian and US Navy aeromagnetic data in the central Arctic seas, *Polarforshcung*, *68*, 35–40.

Glebovsky, V. Y., V. D. Kaminsky, A. N. Minakov, S. A. Merkur'ev, V. A. Childers, and J. M. Brozena (2006), Formation of the Eurasia Basin in the Arctic Ocean as inferred from geohistorical analysis of the anomalous magnetic field, *Geotectonics*, *40*(6), 263–281.

Haq, B. U., J. Hardenbol, and P. R. Vail (1987), Chronology of fluctuating sea levels since the Triassic, *Science*, *235*, 1156–1167.

Hopper, J. R., and W. R. Buck (1996), The effect of lower crustal flow on continental extension and passive margin formation, *J. Geophys. Res.*, *101*, 20,175–20,194.

Jakobsson, M., N. Cherkis, J. Woodward, B. Coakley, and R. Macnab (2000), A new grid of Arctic bathymetry: A significant resource for scientists and mapmakers, *Eos Trans. AGU*, *81*(9), 89.

Jakobsson, M., T. Flodén and the Expedition 302 Scientists (2006), Expedition 302 geophysics: Integrating past data with new results, in *Arctic Coring Expedition (ACEX), Proc. Integr. Ocean Drill. Program*, *302*, doi:10.2204/iodp.proc.302.102.2006.

Jakobsson, M., et al. (2007), The early Miocene onset of a ventilated circulation regime in the Arctic Ocean, *Nature*, *447*, 986–990.

Japsen, P., and P. L. Chalmers (2000), Neogene uplift and tectonics around the North Atlantic: Overview, *Global Planet. Change*, *24*, 165–173.

Japsen, P., J. M. Bonow, P. F. Green, J. A. Chalmers and K. Lidmar-Bergstorm (2006), Elevated, passive continental margins: Long-term highs or Neogene uplifts? New evidence from west Greenland, *Earth Planet. Sci. Lett.*, *248*, 330–339.

Jokat, W. (2005), The sedimentary structure of the Lomonosov Ridge between 88°N and 80°N, *Geophys. J. Int.*, *163*, 698–726.

Jokat, W., and U. Micksch (2004), Sedimentary structure of the Nansen and Amundsen basins, *Arctic Ocean*, *Geophys. Res. Lett.*, *31*, L02603, doi:10.1029/2003GL018352.

Jokat, W., Y. Kristoffersen, and T. M. Rasmussen (1992), Lomonosov Ridge–A double sided continental margin, *Geology*, *20*, 887–890.

Jokat, W., E. Weigelt, Y. Kristoffersen, T. Rasmussen, and T. Schone (1995), New insights into the evolution of the Lomonosov Ridge and the Eurasian Basin, *Geophys. J. Int.*, *122*, 378–392.

Karner, G. D. (1986), Effects of lithospheric in-plane stress on sedimentary basin stratigraphy, *Tectonics*, *5*(4), 573–588.

Kaus, B. P. J., J. A. D. Connolly, Y. Y. Podladchikov, and S. M. Schmalholz (2005), Effect of mineral phase transitions on sedimentary basin subsidence and uplift, *Earth Planet. Sci. Lett.*, *233*, 213–228.

Keen, C. E. (1985), The dynamics of rifting: Deformation of the lithosphere by active and passive driving mechanisms, *R. Astron. Soc. Geophys. J.*, *80*, 95–120.

Kier, G. B., K. Mueller, and T. Rockwell (2001), Origin of regional uplift across southern California and northern Baja California, *Eos Trans. American Geophysical Union*, *82*(47), Fall Meet. Suppl., Abstract T52A-0917.

Kim, B. I., V. V. Verba, V. A. Poselov, M. Y. Sorokin, and W. Jokat (2001), New insights in composition and structure of the sedimentary cover on the Lomonosov Ridge, *Polarforschung*, *68*, 65–70.

Kooi, H., and S. Cloetingh (1989), Intraplate stresses and the tectono-stratigraphic evolution of the central North Sea, *AAPG Mem.*, *48*, 541–558.

Kooi, H., M. Hettema, and S. Cloetingh (1991), Lithosphere dynamics and the rapid Pliocene-Quaternary subsidence phase in the southern north sea basin, *Tectonophysics*, *192*, 245–259.

Kristoffersen, Y., and N. Mikkelsen (2006), On sediment deposition and nature of the plate boundary at the junction between the submarine Lomonosov Ridge, Arctic Ocean and the continental margin of Arctic Canada/north Greenland, *Mar. Geol.*, *225*, 265–278.

Kristoffersen, Y., V. Buratvtsev, W. Jokat, and V. Poselov (1997), Seismic reflection surveys during Arctic Ocean 1996, in *Polarforskningssekretariatet Årsbok 1995/96*, edited by E. Grönlund, pp. 75–77, Polarforskningssekretariatet, Stockholm.

Kristoffersen, Y., H. Berge, and E. Grinheim (2001), An ODP-site survey on Lomonosov Ridge during Arctic Ocean 2001, in *Polarforskningssekretariatet Årsbok 2001*, edited by E. Grönlund, pp. 64–66, Polarforskningssekretariatet, Stockholm.

Kristoffersen, Y., B. Coakley, W. Jokat, M. Edwards, H. Brekke, and J. Gjengedal (2004), Seabed erosion on the Lomonosov Ridge, central Arctic Ocean: A tale of deep draft icebergs in the Eurasia Basin and the influence of Atlantic water inflow on iceberg motion?, *Paleoceanography*, *19*, PA3006, doi:10.1029/2003PA000985.

Kristoffersen, Y., B. J. Coakley, J. K. Hall, and M. Edwards (2007), Mass wasting on the submarine Lomonosov Ridge, central Arctic Ocean, *Mar. Geol.*, *243*, 132–142.

Kusznir, N. J., R. Hunsdalew, and A. M. Roberts (2004), Timing of depth-dependent lithosphere stretching on the S. Lofoten rifted margin offshore mid-Norway: Pre-breakup or post-breakup?, *Basin Res.*, *16*, 279–296.

Langinen, A. E., D. G. Gee, N. N. Lebedeva-Ivanova, and Y. Y. Zamansky (2006), Velocity structure and correlation of the sedimentary cover on the Lomonosov Ridge and in the Amerasian Basin, Arctic Ocean, in *Proceedings of the Fourth International Conference on Arctic Margins: Dartmouth, Nova Scotia, Canada, September 30–October 3, 2003,*

OCS Study MMS 2006-003, edited by and D. Thurston, pp. 179–188, Dep. of the Inter., Anchorage, Alaska.

Langseth, M. G., A. H. Lachenbruch, and B. V. Marshall (1990), Geothermal observations in the Arctic region, in *Geology of North America,* vol. L, *The Arctic Ocean Region*, edited by A. Grantz, L. Johnson, and J. F. Sweeny, pp. 133–151, Geol. Soc. of Am., Boulder, Colo.

Lawver, L. A., A. Grantz, and L. M. Gahagan (2002), Plate kinematic evolution of the present Arctic region since the Ordovician, in *Tectonic Evolution of the Bering Shelf–Chukchi Sea–Arctic Margin and Adjacent Landmasses* [CD-ROM], edited by E. L. A. Miller, A. Grantz, and S.L. Klemperer, *Spec. Pap. Geol. Soc. Am.*, *360*, 333–358.

Leroy, M., F. Gueydan, and O. Dauteuil (2008), Uplift and strength evolution of passive margins inferred from 2-D conductive modeling, *Geophys. J. Int.*, *172*, 464–476.

Leroy, S., et al. (2004), From rifting to spreading in the eastern Gulf of Aden: A geophysical survey of a young oceanic basin from margin to margin, *Terra Nova*, *16*, 185–192.

Mair, J. A., and D. A. Forsyth (1982), Crustal structures of the Canada Basin near Alaska, the Lomonosov Ridge, and adjoining basins near the North Pole, *Tectonophysics*, *89*, 239–254.

McKenzie, D. P. (1978), Some remarks on the development of sedimentary basins, *Earth Planet. Sci. Lett.*, *40*, 25–32.

McNeil, D. H. (1990), Tertiary marine events in the Beaufort-Mackenzie Basin and correlation of Oligocene to Pliocene marine outcrops in Artic North America, *Arctic*, *43*(4), 301–313.

Miller, K. G., M. A. Kominz, J. V. Browning, J. D. Wright, G. S. Mountain, M. E. Katz, P. J. Sugarman, B. S. Cramer, N. Christie-Blick, and S. F. Pekar (2007), The Phanerozoic record of global sea level change, *Science*, *310*, 1293–1298.

Moore, T. C., and the Expedition 302 Scientists (2006), Sedimentation and subsidence history of the Lomonosov Ridge, in *Arctic Coring Expedition (ACEX), Proc. Integr. Ocean Drill. Program*, *302*, doi:10.2204/iodp.proc.302.105.2006.

Moran, K., et al. (2006), The Cenozoic paleoenvironment of the Arctic Ocean, *Nature*, *441*, 601–605.

Peckar, S. F., N. Christie-Blick, M. A. Kominz, and K. G. Miller (2002), Calibration between eustatic estimates from backstripping and oxygen isotope records for the Oligocene, *Geology*, *30*, 903–906.

Polyak, L., M. H. Edwards, B. J. Coakley and M. Jakobsson (2001), Ice shelves in the Pleistocene Arctic Ocean inferred from glaciogenic deep-sea bedforms, *Nature*, *410*, 453–457.

Radionova, E. P., and I. E. Khokhlova (2000), Was the North Atlantic connected with the Tethys via the Arctic in the early Eocene? Evidence from siliceous plankton, in *Early Paleogene Warm Climates and Biosphere Dynamics: Short Papers and Extended Abstracts*, edited by B. Schmitz, B. Sundquist, and F. P. Andreasson, *GFF*, *122*(1), 133–134.

Reemst, P., S. Cloetingh, and S. Fanavoll (1994), Tectono-stratigraphic modeling of Cenozoic uplift and erosion in the south-western Barents Sea, *Mar. Pet. Geol.*, *11*, 478–490.

Ritzmann, O., N. Maercklin, J. I. Faleide, H. Bungum, W. D. Mooney, and T. S. Detweiler (2007), A three-dimensional geophysical model for the Barents Sea region, *Geophys. J. Int.*, *170*, 417–435.

Roberts, A. M., N. J. Kusznir, G. Yielding, and P. Styles (1998), 2D flexural backstripping of extensional basins: The need for a sideways glance, *Pet. Geosci.*, *4*, 327–338.

Rohrman, M., and P. A. van der Beek (1996), Cenozoic postrift domal uplift of North Atlantic margins; an asthenospheric diapirism model, *Geology*, *24*, 901–904.

Sangiorgi, F., H.-J. Brumsack, D. A. Willard, H. Brinkhuis, S. Schouten, C. E. Stickley, M. O'Regan, G.-J. Reichart, J. S. Sinninghe Damsté, and H. Brinkhuis (2008), A ~26 million year gap in the central Arctic record at the greenhouse-icehouse transition: Looking for clues, *Paleoceanography*, *23*, PA1S04, doi:10.1029/2007PA001477.

Skelton, A., and M. Jakobsson (2007), Could peridotite hydration reactions have provided a contributory driving force for Cenozoic uplift and accelerated subsidence along the margins of the North Atlantic and Labrador Sea?, *Norw. J. Geol.*, *87*, 241–248.

Sluijs, A., et al. (2006), Subtropical Arctic Ocean temperatures during the Paleocene/Eocene thermal maximum, *Nature*, *441*, 610–613.

Sluijs, A., U. Röhl, S. Schouten, H.-J. Brumsack, F. Sangiorgi, J. S. Sinninghe Damsté, and H. Brinkhuis (2008), Arctic late Paleocene–early Eocene paleoenvironments with special emphasis on the Paleocene-Eocene thermal maximum (Lomonosov Ridge, Integrated Ocean Drilling Program Expedition 302), *Paleoceanography*, *23*, PA1S11, doi:10.1029/2007PA001495.

Steckler, M. S. (1985), Uplift and extension at the Gulf of Suez: Indications of induced mantle convection, *Nature*, *317*, 135–139.

Stein, R., B. Boucsein, and H. Meyer (2006), Anoxia and high primary production in the Paleogene central Arctic Ocean: First detailed records from Lomonosov Ridge, *Geophys. Res. Lett.*, *33*, L18606, doi:10.1029/2006GL026776.

Stickley, C., N. Koç, H.-J. Brumsack, R. W. Jordan, and I. Suto (2008), A siliceous microfossil view of middle Eocene Arctic paleoenvironments: A window of biosilica production and preservation, *Paleoceanography*, doi:10.1029/2007PA001485, in press.

Sweeney, J. F., J. R. Weber, and S. M. Blasco (1982), Continental ridges in the Arctic Ocean: LOREX constraints, *Tectonophysics*, *89*, 217–237.

Tang, J., and I. Lerche (1992), Tertiary flexural evolution of the Beaufort-McKenzie Basin, Canada, *Mar. Pet. Geol.*, *9*, 245–255.

Tsikalas, F., J. I. Faleide, O. Eldholm, and J. Wilson (2005), Late Mesozoic-Cenozoic structural and stratigraphic correlations between the conjugate mid-Norway and NE Greenland continental margins, in *Petroleum Geology: North-West Europe and Global Perspectives—Proceedings of the 6th Petroleum Geology Conference*, vol. 2, edited by A. G. Doré and B. Vining, pp. 785–801, Geol. Soc., London.

van Balen, R. T., Y. Y. Podladchikov, and S. A. P. L. Cloetingh (1998), A new multilayered model for intraplate stress-induced differential subsidence of faulted lithosphere, applied to rifted basins, *Tectonics*, *17*(6), 938–954.

van Wees, J. D., and S. Cloetingh (1996), 3D flexure and intraplate compression in the North Sea Basin, *Tectonophysics*, *266*, 343–359.

Vogt, P. R., P. T. Taylor, L. C. Kovacs, and G. L. Johnson (1979), Detailed aeromagnetic investigation of the Arctic Basin, *J. Geophys. Res.*, *84*, 1071–1089.

Watts, A. B. (2001), *Isostacy and Flexure of the Lithosphere*, Cambridge Univ. Press, Cambridge, U. K.

Weber, J. R. (1979), The Lomonosov Ridge experiment: 'LOREX 79,' *Eos Trans. AGU*, *60*(42), 715.

Weber, J. R., and J. F. Sweeney (1985), Reinterpretation of morphology and crustal structure in the central Arctic Ocean, *J. Geophys. Res.*, *90*, 663–677.

Weber, J. R., and J. F. Sweeney (1990), Ridges and basins in the central Arctic Ocean, in *Geology of North America,* vol. L, *The Arctic Ocean Region*, edited by A. Grantz, L. Johnson, and J. F. Sweeny, pp. 305–336, Geol. Soc. of Am., Boulder, Colo.

Weigelt, E., and W. Jokat (2001), Peculiarities of roughness and thickness of oceanic crust in the Eurasian Basin, Arctic Ocean, *Geophys. J. Int.*, *145*, 505–516.

Weissel, J. K., and G. D. Karner (1989), Flexural uplift of rift flanks due to tectonic denundation of the lithosphere during extension, *J. Geophys. Res.*, *94*, 13,919–13,950.

Whitmarsh, R. B., and P. R. Miles (1995), Models of the development of the west Iberia rifted continental margin at 40°30′N deduced from surface and deep-tow magnetic anomalies, *J. Geophys. Res.*, *100*, 3789–3806.

Whitmarsh, R. B., L. M. Pinheiro, P. R. Miles, and M. Recq (1993), Thin crust at the western Iberia ocean-continent transition and ophiolites, *Tectonics*, *12*(5), 1230–1239.

Whitmarsh, R. B., G. Manatschal, and T. Minshull (2001), Evolution of magma-poor continental margins from rifting to seafloor spreading, *Nature*, *413*, 150–154.

Worsley, D. (2006), The post-Caledonian geological development of Svalbard and the Barents Sea, *NGF Abstr. Proc.*, *3*, 5–21.

Young, F. G., and D. H. McNeil (1984), Cenozoic stratigraphy of the Mackenzie Delta, Northwest Territories, *Bull. Geol. Surv.*, 336.

Zarkhidze, V. S. (1992), Paleogene and Neogene history of Arctic Ocean evolution (in Russian), in *Geologic History of the Arctic in the Mesozoic and Cenozoic*: *Proceedings of the V.N. Saks Conference*, vol. 2. pp. 6–28, VNII Okeangeol., St. Petersburg, Russia.

Ziegler, A. P., and S. Cloetingh (2004), Dynamic processes controlling evolution of rifted basins, *Earth Sci. Rev.*, *64*, 1–50.

J. Backman, M. Jakobsson, and A. Skelton, Department of Geology and Geochemistry, Stockholm University, S-10691 Stockholm, Sweden.

H. Brinkhuis and F. Sangiorgi, Palaeoecology, Laboratory of Palaeobotany and Palynology, Institute of Environmental Biology, Utrecht University, Budapestlaan 4, NL-3584 CD Utrecht, Netherlands.

H.-J. Brumsack, Institut für Chemie und Biologie des Meeres, Oldenburg University, Oldenburg, D-26111, Germany.

N. Koç and C. Stickley, Polar Environmental Centre, Norwegian Polar Institute, N-9296 Tromsø, Norway.

K. Moran, M. O'Regan, and R. Pockalny, Graduate School of Oceanography, University of Rhode Island, Narragansett, RI 02882, USA. (oregan@gso.uri.edu)

D. Willard, U.S. Geological Survey, MS 926A, Reston, VA 20192, USA.